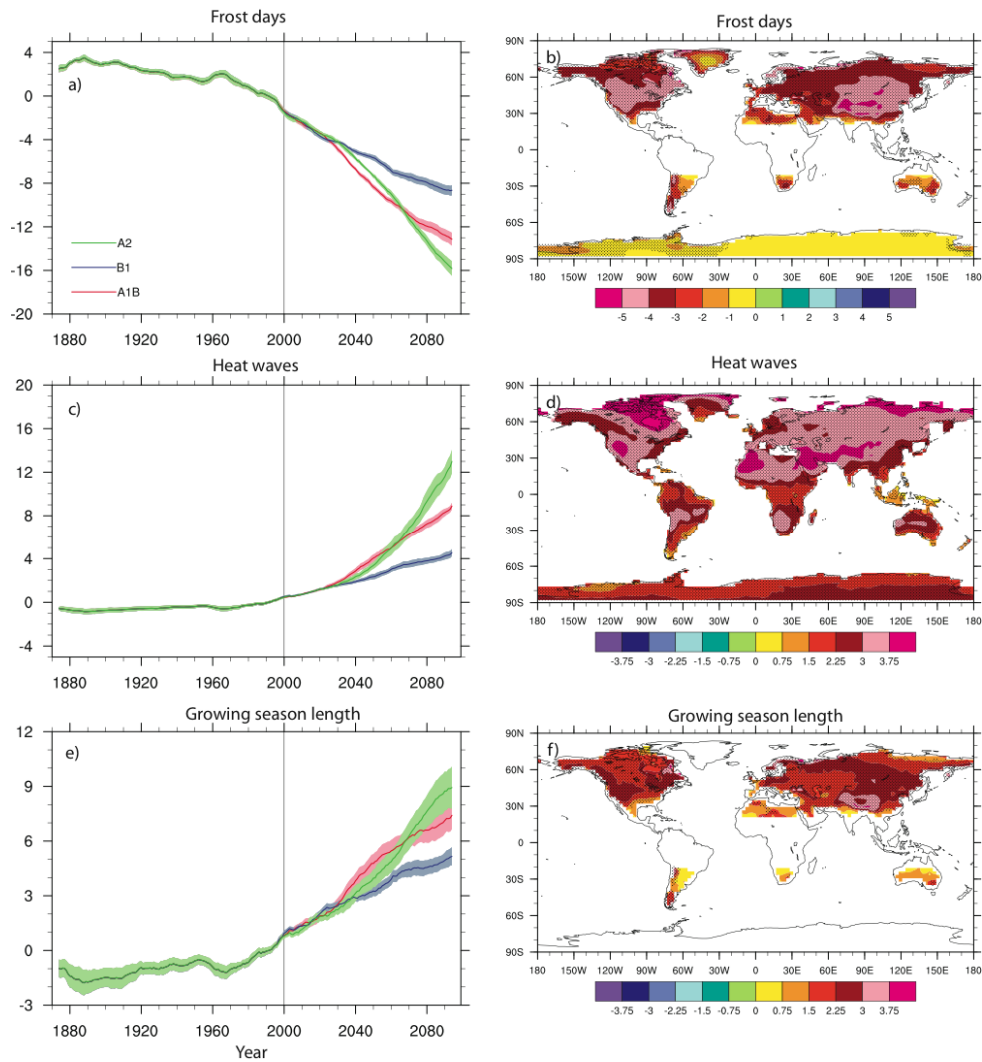


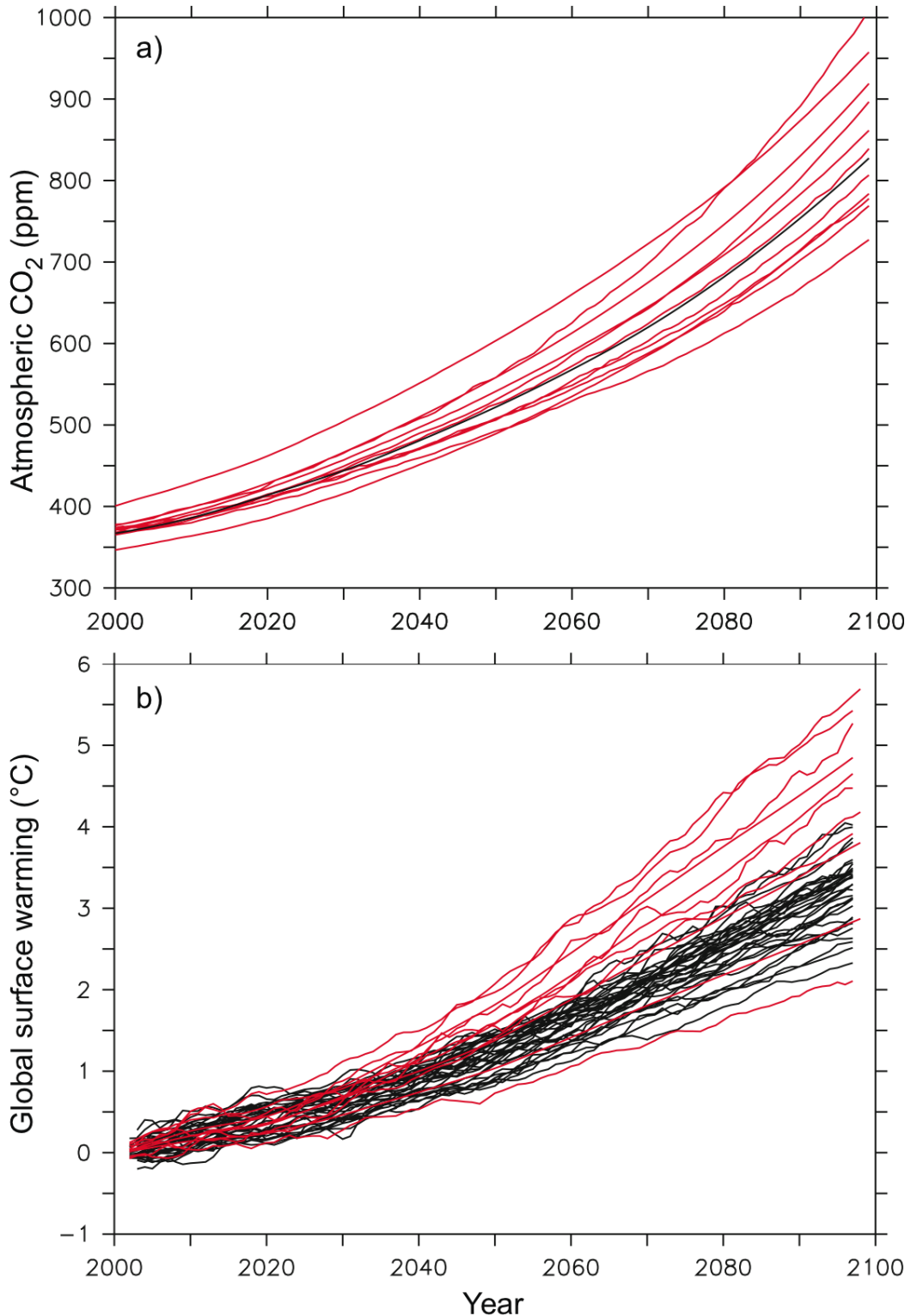
1
2



3
4

Figure 10.3.17. Changes in extremes based on multi-model simulations from nine global coupled climate models, adapted from Tebaldi et al. (2006). a) Globally averaged changes in frost days (the frost day index is defined as the total number of days in a year with absolute minimum temperature below 0°C) for a low (SRES B1), middle (SRES A1B), and high (SRES A2) scenario. b) changes of spatial patterns of frost days based on simulations between two 20-year means (2080–2099 minus 1980–1999) for the A1B scenario. c) Globally averaged changes in heat waves (a heat wave is defined as the longest period in the year of at least 5 consecutive days with maximum temperature at least 5°C higher than climatology of the same calendar day). d) changes of spatial patterns of heat waves based on simulations between two 20-year means (2080–2099 minus 1980–1999) for the A1B scenario. e) Globally averaged changes growing season length (the growing season is defined as the length of the period between the first spell of five consecutive days with mean temperature above 5°C and the last such spell of the year). f) changes of spatial patterns of growing season length based on simulations between two 20-year means (2080–2099 minus 1980–1999) for the A1B scenario. Solid lines in panels a, c and e are the 10-year smoothed multi-model ensemble means, the envelope indicates the ensemble mean standard deviation. Stippling in panels b, d and f denote areas where at least 5 of the 9 models concur in determining that the change is statistically significant. Extreme indices are calculated only over land. Frost days and growing season are only calculated in the extratropics. Extremes indices are calculated following Frich et al. (2002). Each model's timeseries has been centered around its 1980–1999 average and normalized (rescaled) by its standard deviation computed (after detrending) over the period 1960–2099, then the models were aggregated into an ensemble average, both at the global average and at the grid-box level. Thus, changes are given in units of standard deviations.

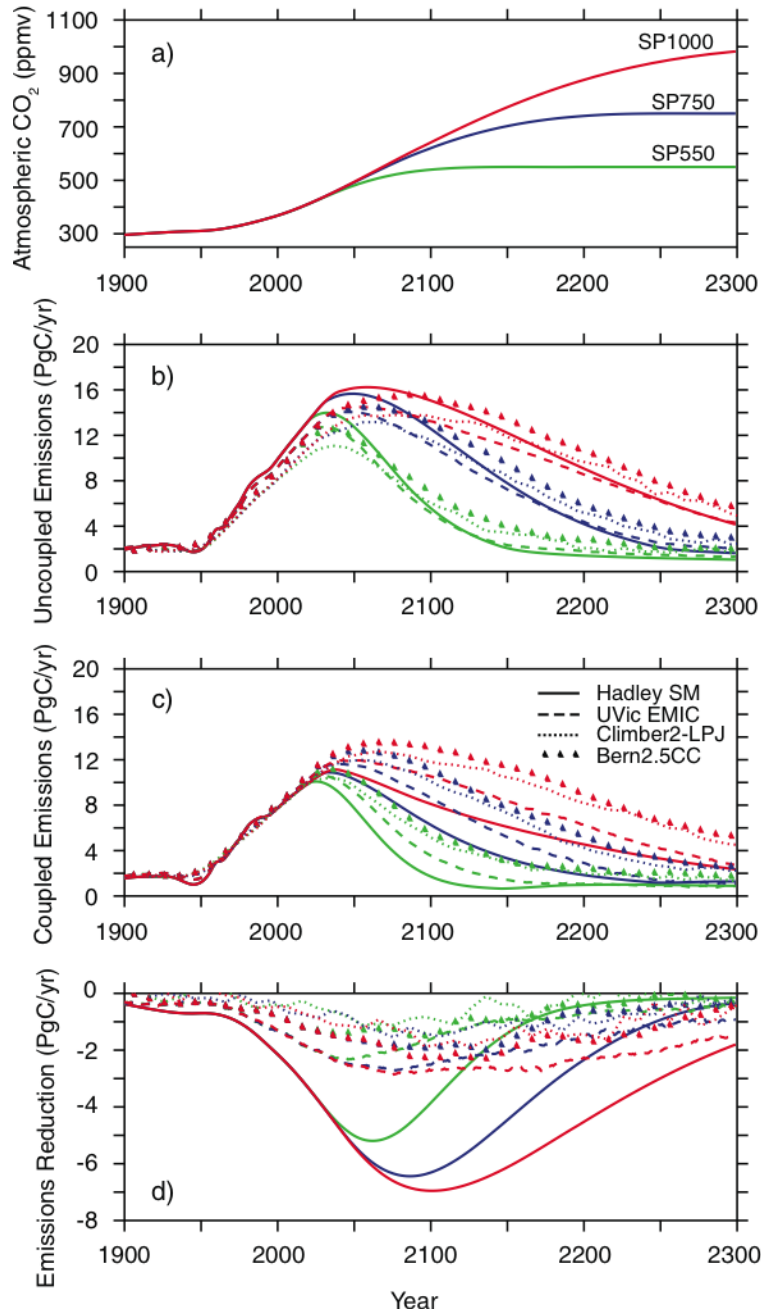
1
2



3
4
5
6
7
8
9
10
11
12

Figure 10.4.1. a) 21st century atmospheric CO₂ concentration as simulated by the 11 C4MIP models for the SRES A2 emission scenario (red) compared with the standard atmospheric CO₂ concentration used as a forcing for many IPCC-AR4 climate models. The standard CO₂ concentration values were calculated by the BERN-CC model and are identical to the TAR. For some IPCC-AR4 models, different carbon cycle models were used to convert carbon emissions to atmospheric concentrations; b) Same for the global averaged surface temperature change. The C4MIP global temperature change has been corrected to account for the non-CO₂ radiative forcing used by the standard IPCC-AR4 climate models.

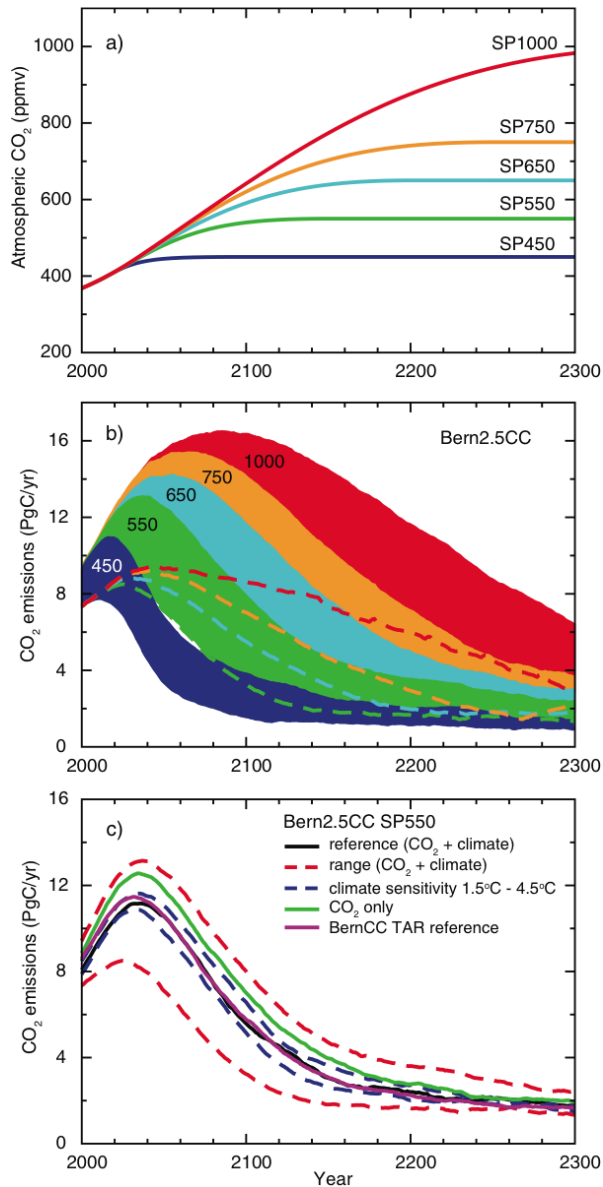
1
2



3
4
5
6
7
8
9
10
11
12

Figure 10.4.2. a) Atmospheric CO₂ stabilization scenarios, SP1000 (red), SP750 (blue) and SP550 (green). b) Compatible annual emissions calculated by four models, Hadley simple model (Huntingford and Cox, 2000) (solid), UVic EMIC (Matthews, 2005)(dash), Climber2-LPJ (dotted) and BERN2.5CC EMIC (Joos et al., 2001; Plattner et al., 2001) (triangles) for the three stabilization scenarios without accounting for the impact of climate on the carbon cycle. c) Same as b) but when the climate impact on the carbon cycle is accounted for. d) Difference between b) and c) showing the impact of the climate-carbon cycle feedback on the calculation of compatible emissions.

1
2



3
4
5
6
7
8
9
10
11
12
13
14

Figure 10.4.3. Projected CO₂ emissions leading to stabilization of atmospheric CO₂ concentrations at different levels and the effect of uncertainty in carbon cycle processes on calculated emissions. Panel a) shows the assumed trajectories of CO₂ concentration (SP scenarios)(Knutti et al., 2005); b) and c) show the implied CO₂ emissions, as projected with the Bern2.5CC carbon cycle model of intermediate complexity (Joos et al., 2001; Plattner et al., 2001). The ranges given in b) for each of the SP scenarios represent effects of different model parameterizations and assumptions illustrated for scenario SP550 in panel c) (range for "CO₂ +climate"). The upper and lower bounds in b) are indicated by the top and bottom of the shaded areas. Alternatively, the lower bound (where hidden) is indicated by a dashed line. Panel c) illustrates emission ranges and sensitivities for scenario SP550.

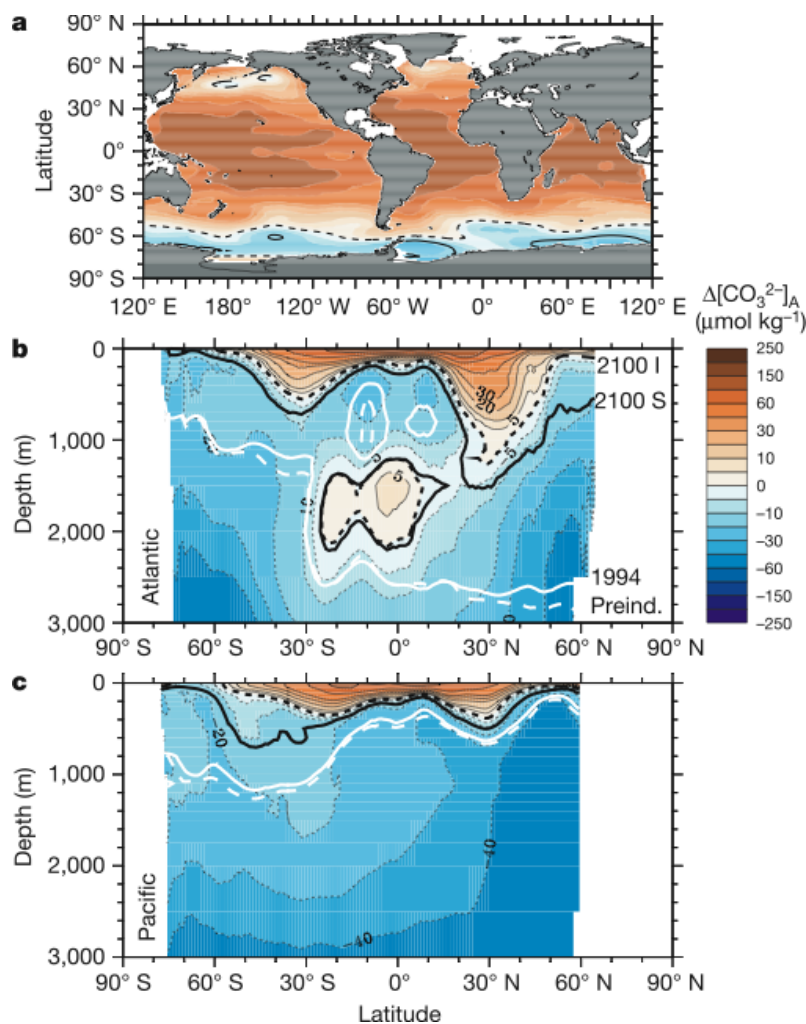
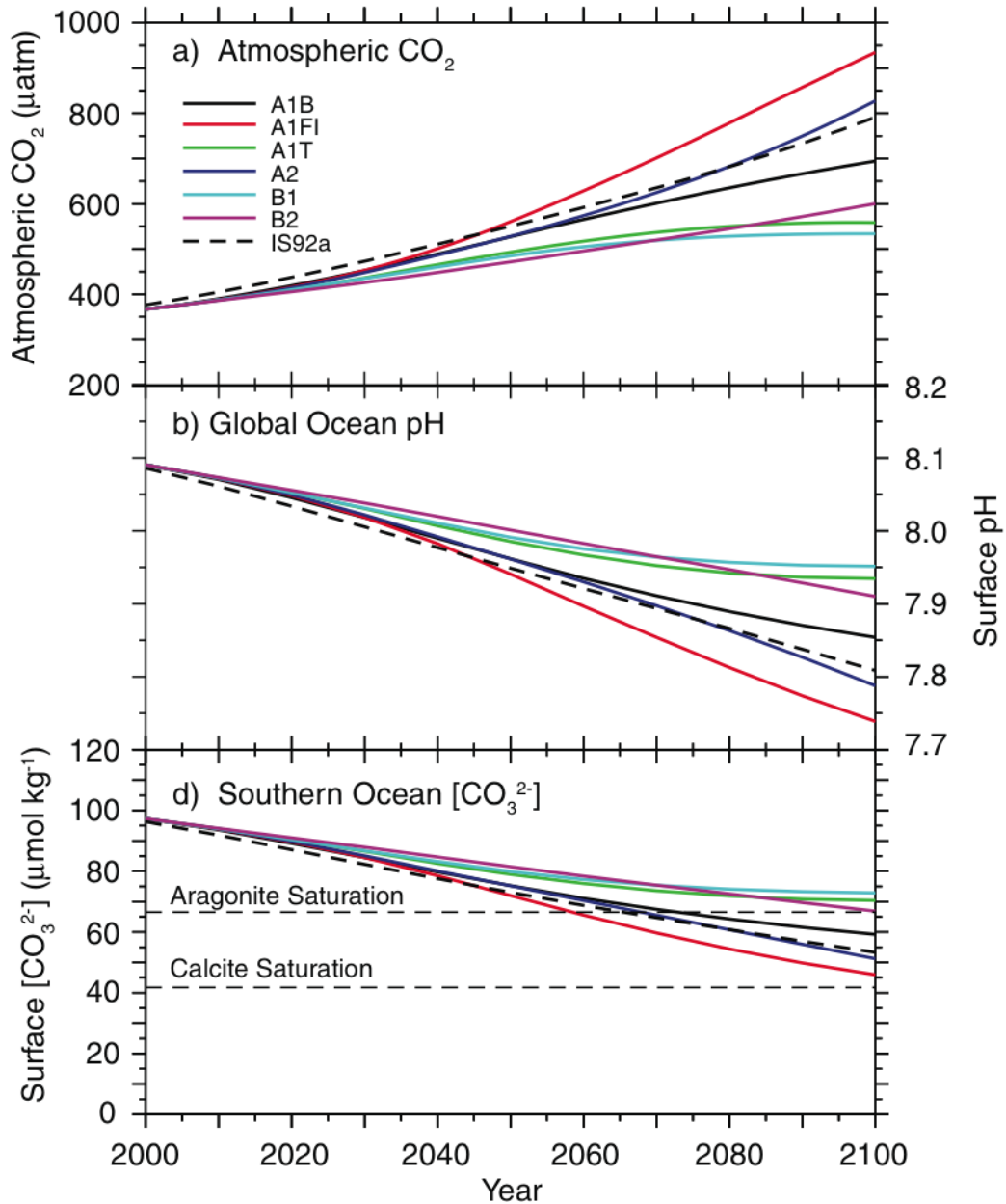
1
23
4
5
6
7
8
9
10
11
12

Figure 10.4.4. Aragonite supersaturation state in the year 2100. The aragonite supersaturation is the in situ carbonate ion concentration minus that for aragonite-equilibrated sea water at the same salinity, temperature and pressure. Shown are the OCMIP-2-model median concentrations in the year 2100 under scenario IS92a: a) surface map; b) Atlantic; and c) Pacific zonal averages. Thick lines indicate the aragonite saturation horizon in 1765 (Preindustrial, white dashed line), 1994 (white solid line) and 2100 (black solid line for S650; black dashed line for IS92a). Positive values indicate supersaturation; negative values indicate undersaturation. From (Orr et al., 2005).

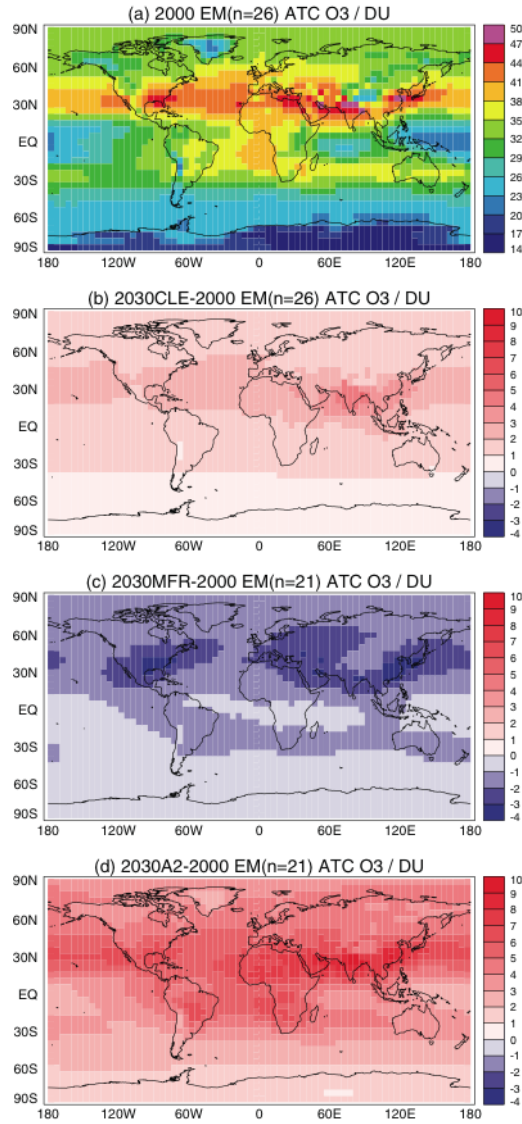
1
2



3
4
5
6
7
8
9
10

Figure 10.4.5. Global average surface pH changes and carbonate ion concentration in the Southern Ocean under various SRES scenarios. Time series of a) atmospheric CO₂ for the six illustrative IPCC SRES scenarios, b) projected global average surface pH changes, and c) projected average surface carbonate ion concentration in the Southern Ocean for the BERN2.5D EMIC (Plattner et al., 2001). The results for the SRES scenarios A1T and A2 are similar to those for the non-SRES scenarios S650 and IS92a, respectively. Modified from (Orr et al., 2005).

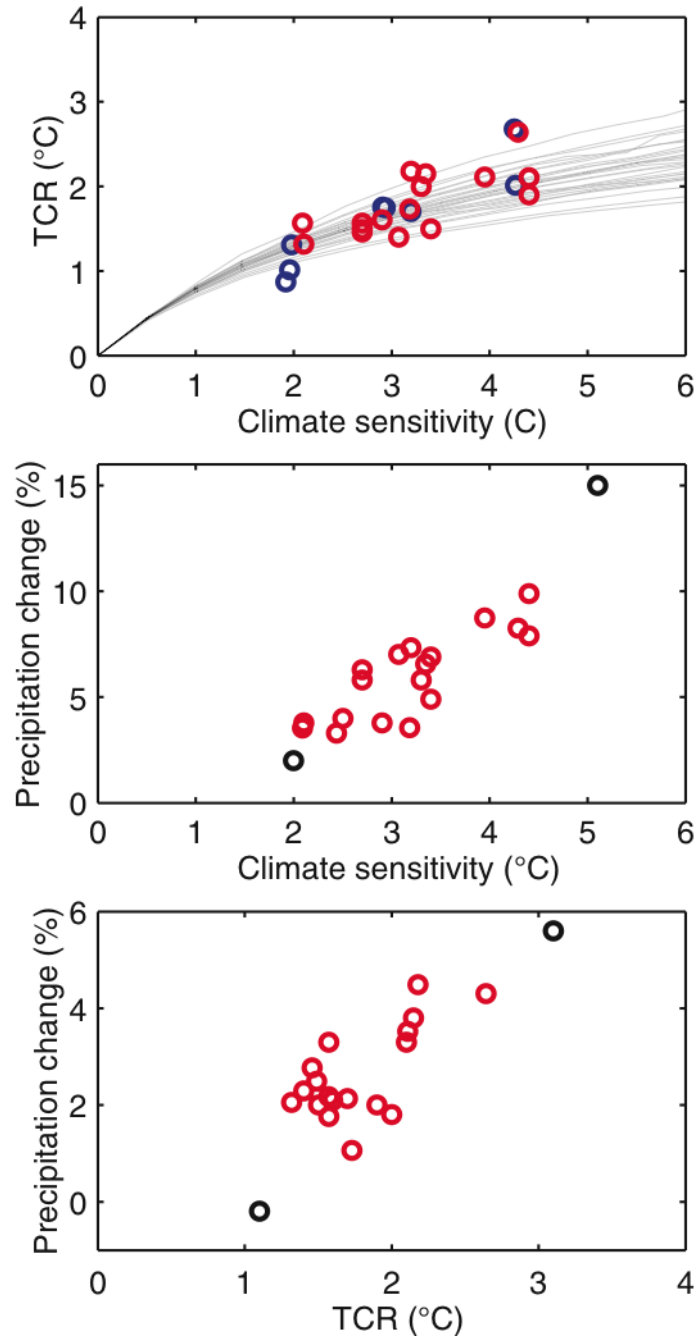
1
2



3
4
5
6
7
8
9
10
11

Figure 10.4.6. Tropospheric ozone simulated in the ACCENT model intercomparison (Stevenson et al., 2006). The panels in the figure show annual mean tropospheric column results (in units of DU). Each panel is a multi model ensemble mean; the number of models in the ensemble is given in brackets. (a) Year 2000; (b) difference between 2030CLE (IIASA Current Legislation) scenario and 2000; (c) difference between 2030MFR (IIASA Maximum Feasible Reductions) and 2000; and (d) difference between 2030A2 (SRES A2) and 2000.

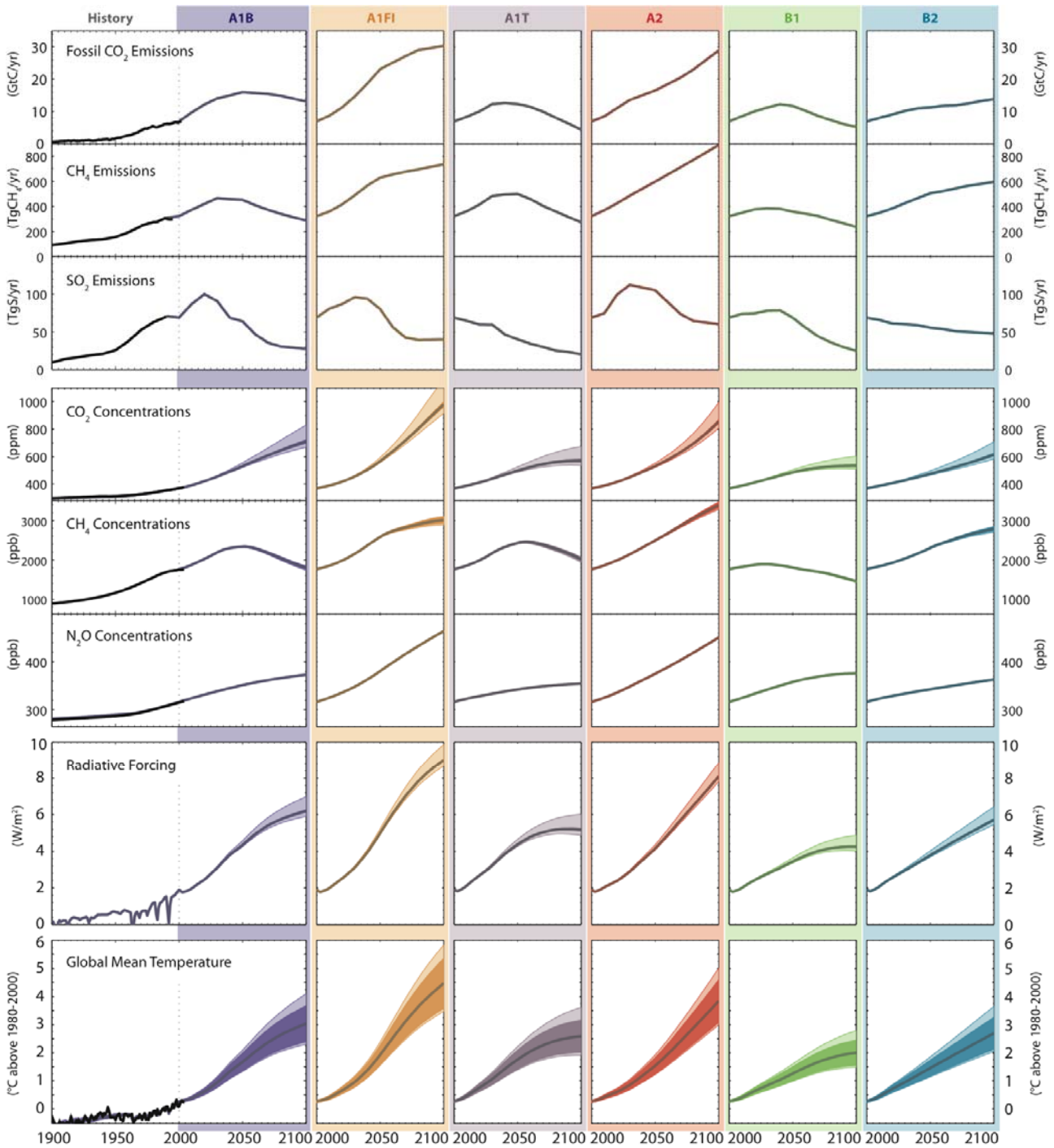
1
2



3
4
5
6
7
8
9
10
11
12

Figure 10.5.1. a) TCR versus equilibrium climate sensitivity for all AOGCMs (red dots), EMICs (blue dots) and from a large ensemble of the Bern2.5D EMIC (Knutti et al., 2005) using different ocean vertical diffusivities and mixing parameterizations (black lines). b) Global mean precipitation change (%) as a function of global mean temperature change at equilibrium for doubling atmospheric CO₂ in slab ocean GCMs, c) Global mean precipitation change (in %) as a function of global mean temperature change (TCR) in a transient 1%/yr CO₂ increase scenario at the time of doubling, simulated by coupled AOGCMs. Black circles in b and c mark ranges covered by the TAR AOGCMs for each quantity.

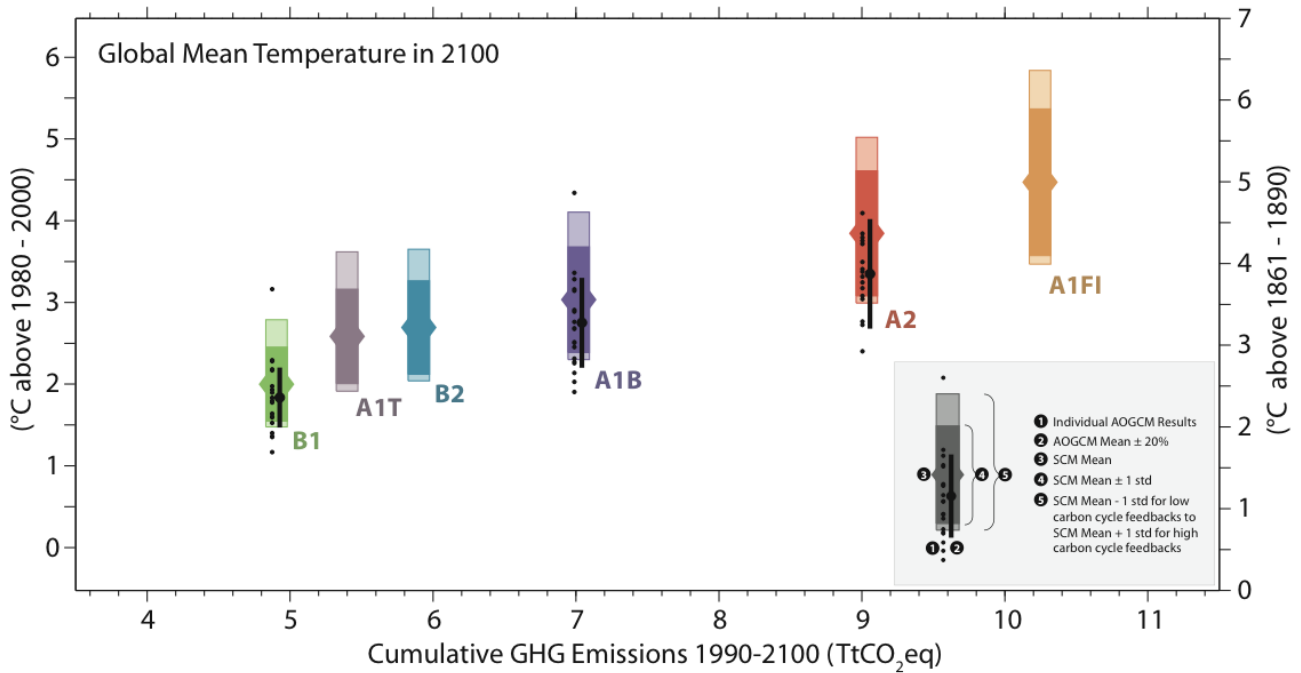
1
2



3
4
5
6
7
8
9
10
11
12
13
14
15
16

Figure 10.5.2. Fossil CO₂, CH₄, and SO₂ emissions for six illustrative SRES non-mitigation emission scenarios, their corresponding CO₂, CH₄, and N₂O concentrations, radiative forcing and global mean temperature projections based on a simple climate model tuned to nineteen AOGCMs. The dark shaded areas in the bottom temperature panel represent the mean ± 1 standard deviation for the nineteen model tunings. The lighter shaded areas depict the change in this uncertainty range, if carbon cycle feedbacks are assumed to be lower or higher than in the medium setting. Mean projections for mid carbon cycle assumptions for the six illustrative SRES scenarios are shown as thick colored lines. Historical emissions are shown for fossil and industrial CO₂ (Marland et al., 2005), for SO₂ (van Aardenne et al., 2001) and CH₄ (van Aardenne et al., 2001), adjusted to (Olivier and Berdowski, 2001)). Observed CO₂, CH₄, and N₂O concentrations are as presented in Chapter 6. Global mean temperature results from the simple climate model for anthropogenic and natural forcing compare favourably with 20th century observations as shown in the lower left panel (Folland et al., 2001; Jones et al., 2001; Jones and Moberg, 2003)

1
2



3
4
5
6
7
8
9
10
11
12
13
14
15
16
17

Figure 10.5.3. Global mean temperature projections using a simple climate model for the year 2100 for the six illustrative SRES non-mitigation scenarios. The scenarios are ordered by their cumulative greenhouse gas (GHG) emissions from 1990 to 2100 (see text). Both the magnitude of the projected warming and its uncertainty range generally increase for higher cumulative GHG emissions, although differences in gas-by-gas emission ratios, aerosol emissions and the timing of emissions can modulate this relationship. The coloured dark shaded bars are the simple climate model uncertainty ranges (mean \pm one standard deviation) for mid carbon cycle settings. The lower (upper) bound of the light shaded bars is the corresponding lower (upper) bound of the one standard deviation uncertainty range for low (high) carbon cycle settings, as in Figure 10.5.2. Up to 21 AOGCMs were run for the scenarios B1, A1B and A2. Their projected warming by 2090–2100 is shown here for comparison (small black dots). The projected AOGCM mean warming \pm 20% of the temperature change, for the period 2090–2100, is indicated by the vertical black lines (see Figure 10.5.7 for other probabilistic estimates of uncertainty).

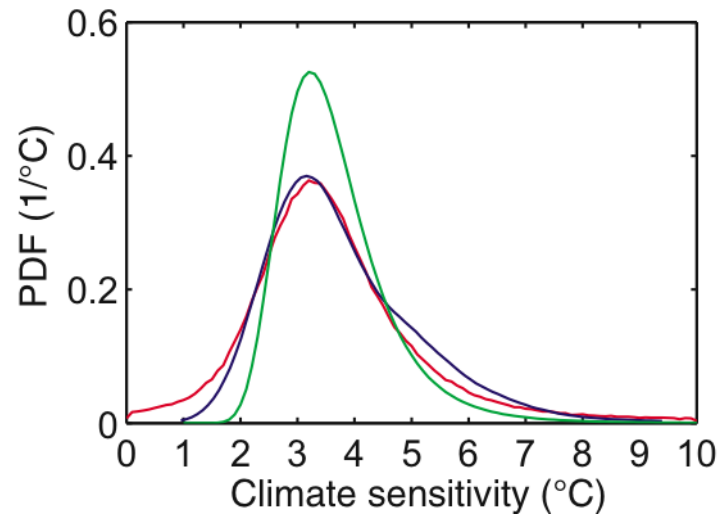
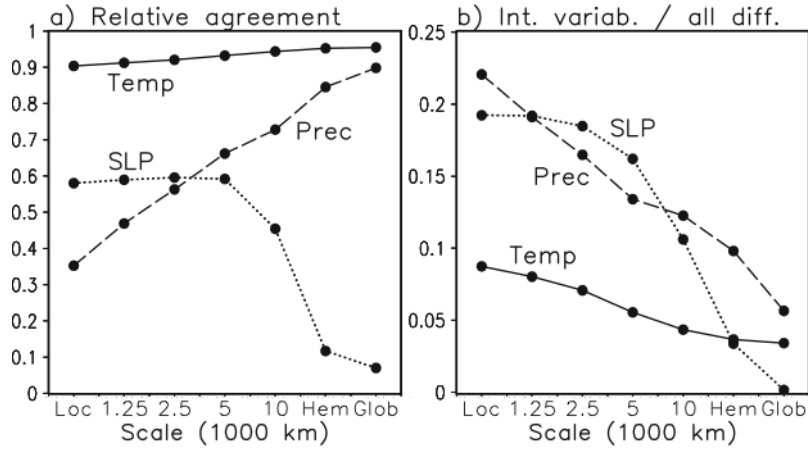
1
23
4
5
6
7
8

Figure 10.5.4. PDFs of climate sensitivity based on climate model agreement with present day climatology, from Murphy et al. (2004) (green), Piani et al. (2005) (blue) and Knutti et al. (2006) (red). PDFs are truncated at 10°C.

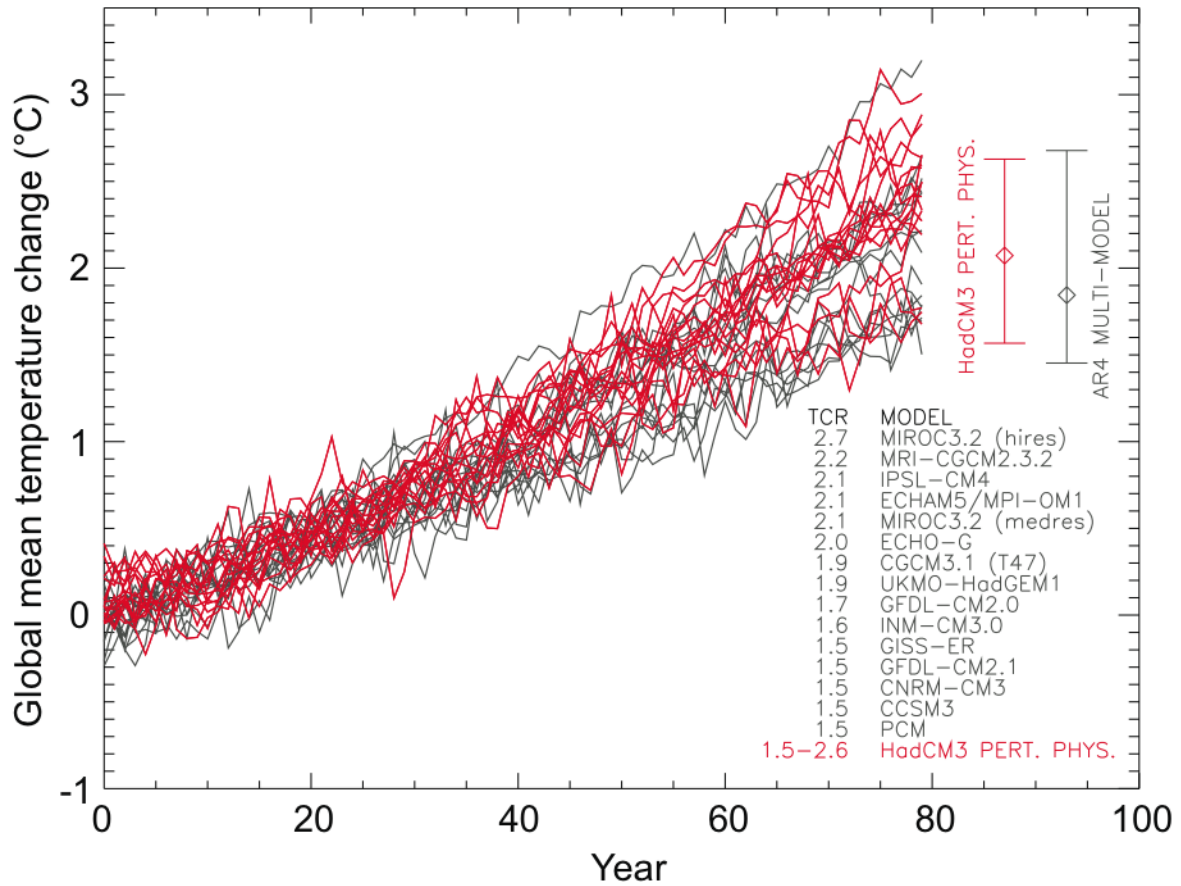
1
2



3
4
5
6
7
8
9
10
11
12

Figure 10.5.5. Statistics of annual mean responses to the SRES A1B scenario, for 2080–2099 relative to 1980–1999, calculated from the 21 member AR4 multi model ensemble using the methodology of Räisänen (2001). Results are expressed as a function of horizontal scale (“Loc” = gridbox scale; “Hem” = hemispheric scale; “Glob” = global mean): (a) The relative agreement between ensemble members, defined as the square of the ensemble-mean response (corrected to avoid sampling bias) divided by the mean squared response of individual ensemble members; (b) The contribution of internal variability to the ensemble variance of responses. Values are shown for surface air temperature, precipitation and sea level pressure.

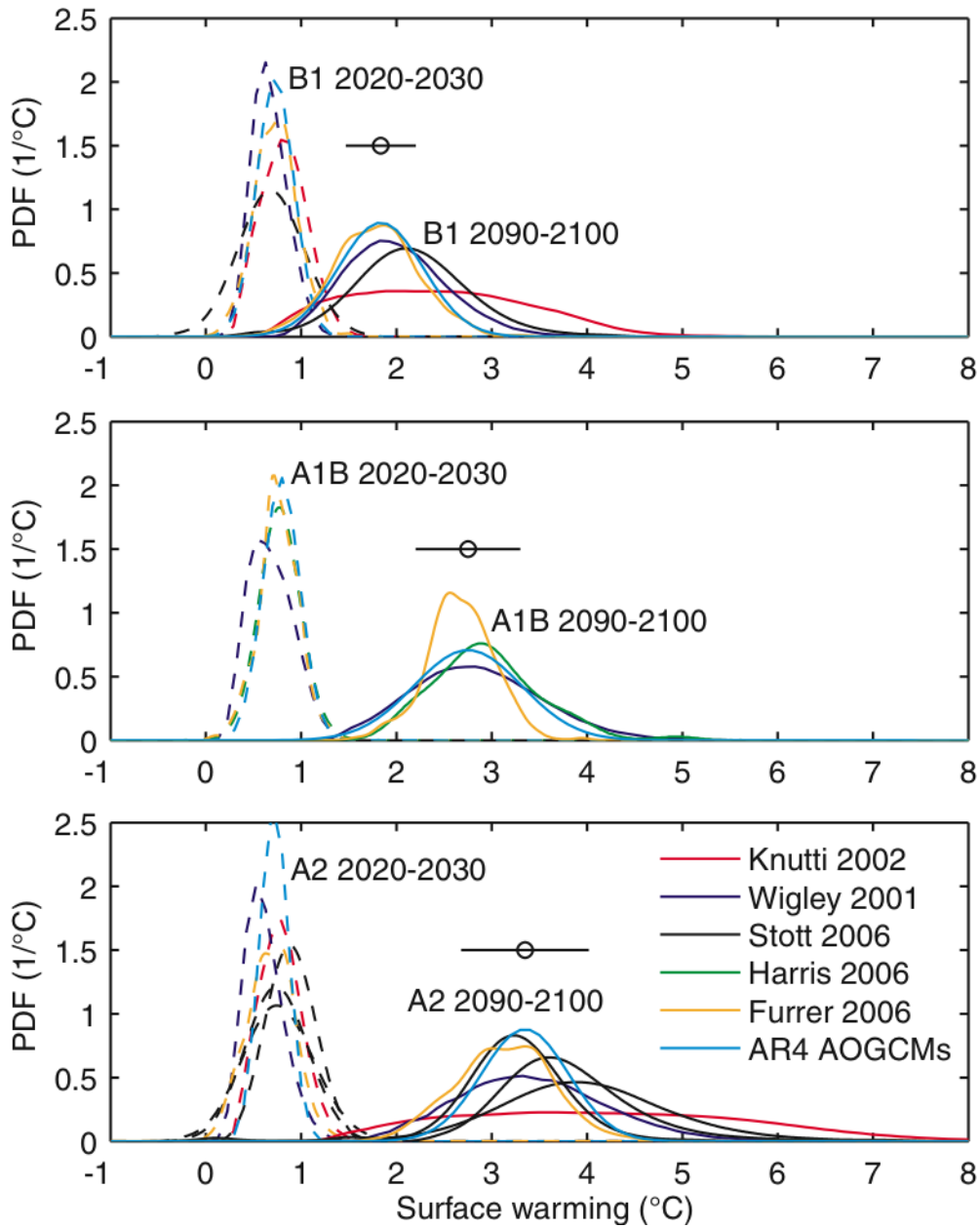
1
2



3
4
5
6
7
8
9
10
11
12
13

Figure 10.5.6. Response of global mean surface air temperature to a 1% per year increase in CO₂ from 17 member ensembles constructed from versions of the HadCM3 coupled ocean-atmosphere model with multiple perturbations to uncertain surface and atmospheric parameters (red lines) and coupled models comprising the AR4 multi-model ensemble (grey lines). The mean and range of Transient Climate Response (TCR) for the two ensembles is indicated by the vertical bars and the table shows TCR values for multi-model ensemble members compared with the range from the HadCM3 perturbed physics ensemble. For the UKMO-HadGEM1 and MIROC3.2 hires models, only the scenario in which CO₂ concentrations are held fixed after year 70 were available, resulting in a likely but small underestimation of the model TCR.

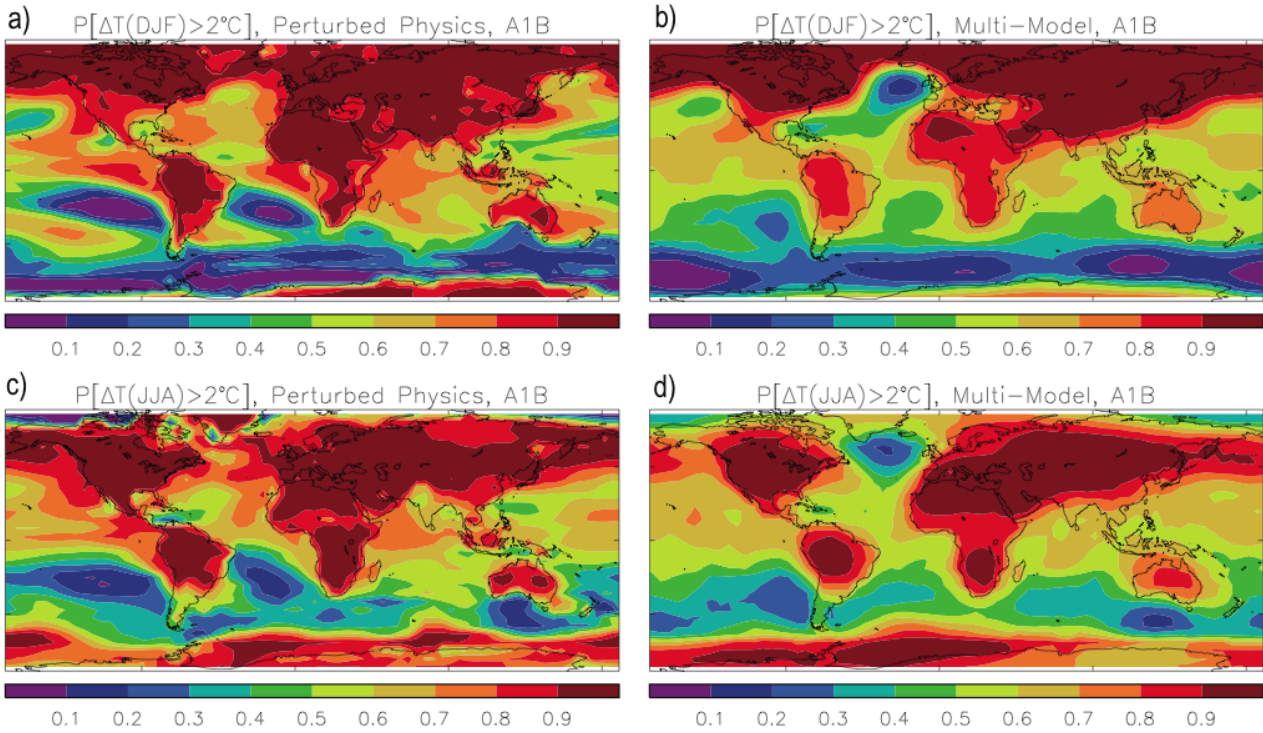
1
2
3



4
5
6
7
8
9
10
11
12
13
14

Figure 10.5.7. Probability density functions from different studies for global mean temperature change for the SRES scenarios B1, A1B and A2 and for the decades 2020–2030 and 2090–2100 relative to the 1980–2000 average (Wigley and Raper, 2001; Knutti et al., 2002; Furrer et al., 2006; Harris et al., 2006; Stott et al., 2006). A normal distribution fitted to the multi-model ensemble is given for comparison. The horizontal bars denote the AOGCM mean plus minus 20%, the same quantity as shown in Figure 10.5.3 where the AOGCM uncertainty is compared with the simple model results. This range approximately covers the one standard deviation uncertainty derived from the AOGCMs and in contrast to the fitted AOGCM distributions accounts for the fact that the number of models available for each scenarios and is different.

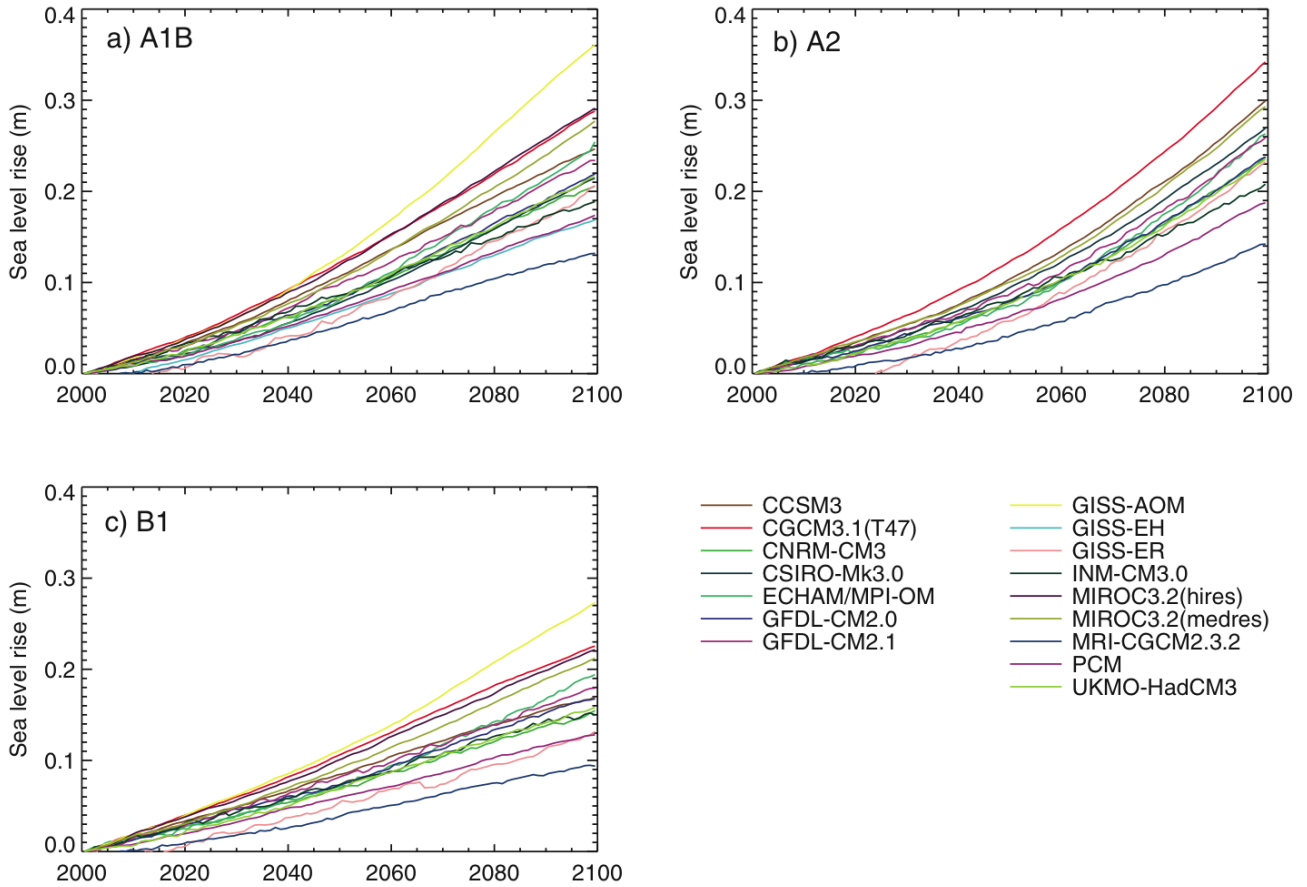
1
2



3
4
5
6
7
8
9
10

Figure 10.5.8. Estimated probabilities for a mean surface temperature change exceeding 2°C under the SRES A1B scenario, for 2080–2099 relative to 1980–1999. Results obtained from a perturbed physics ensemble of a single model (panels a and c), based on Harris et al. (2006), are compared against results from the AR4 multi model ensemble (panels b and d), based on Furrer et al. (2006)), for December-February (DJF, panels a and b) and June-August (JJA, panels c and d).

1
2



3
4
5
6
7

Figure 10.6.1. Projected global average sea level rise (m) due to thermal expansion during the 21st century relative to 2000 under SRES scenarios a) A1B, b) A2 and c) B1.